Lateral Dynamics of Flexible Rotors Supported by Controllable Gas Bearings Theory & Experiment

Pierart Vásquez, Fabián Gonzalo; Santos, Ilmar

Published in:
Proceedings of the 11th International Conference on Vibrations in Rotating Machines

Publication date:
2015

SIRM 2015 – 11th International Conference on Vibrations in Rotating Machines,
Magdeburg, Deutschland, 23. – 25. February 2015

Lateral Dynamics of Flexible Rotors Supported by Controllable Gas Bearings Theory & Experiment

Fabian G. Pierart [1], **Ilmar F. Santos** [2]

[1] Department of Mechanical Engineering, Technical University of Denmark, Lyngby, Denmark, fpvas@mek.dtu.dk
[2] Department of Mechanical Engineering, Technical University of Denmark, Lyngby, Denmark, ifs@mek.dtu.dk

Abstract

Active gas bearings might represent a mechatronic answer to the growing industrial need for high performance turbomachinery. In this framework, the paper gives a theoretical and experimental contribution to the improvement of lateral dynamics of rotating machines. The work aims at demonstrating theoretically as well as experimentally the feasibility of applying active lubrication to gas journal bearings. The operation principle is to generate active forces by regulating the radial injection of a compressible lubricant (gas) by means of piezoelectric actuators mounted on the back of the bearing sleeve. The active control principle is built using eddy-current sensor signals to detect the lateral motion of the rotor. A feedback law is used to couple the lateral dynamics of a flexible rotor-bearing system with the pneumatic and dynamic characteristics of a piezoelectric actuated valve system. A proportional derivative (PD) control is designed based on a theoretical model and experimentally validated. Results show the considerable performance advantages of such a type of controllable bearing. Discrepancies between theoretical and experimental results are elucidated in the paper, considering some simplifying assumptions used to derive the control matrix.

Nomenclature

C_d	Coefficient of discharge [-]
$\mathbf{A}$	System matrix
$\mathbf{B}$	Input matrix
$\mathbf{C}$	Output matrix
$\mathbf{D}$	Damping matrix [Ns/m]
$\mathbf{F}$	External forces matrix [N]
$\mathbf{G}$	Gyroscopic matrix [Kg m]
$\mathbf{K}$	Stiffness matrix [N/m]
$\mathbf{M}$	Mass matrix [Kg]
$\mathbf{Q}$	Generic force matrix [N]
$\mathbf{q}$	Generic coordinate vector for the rotor bearing FE model
$\mathbf{u}$	Input voltage signal [V]
$\mathbf{z}$	Generic coordinate vector in state space form
μ	Fluid viscosity [Pa s]
Ω	Angular velocity [rad/s]
ω	Excitation frequency [rad/s]
ε	Damping factor [-]
d	Orifice diameter function [m]
d_0	Orifice external diameter [m]
d_{int}	Orifice internal diameter [m]
e	Error [m]
h	Fluid film thickness [m]
i	Complex number [-]
K_d	Derivative gain [Vs/m]
K_p	Proportional gain [V/m]
L	Bearing length [m]
N	Cut-off frequency constant [Hz]
p	Fluid film pressure [Pa]
R	Bearing radius [m]
s	Laplace operator [-]
t	Time [s]
U	Journal peripheral linear velocity [m/s]
V_{inj}	Fluid injection velocity [m/s]
x	Radial coordinate [m]
y	Circumferential coordinate [m]
z	Axial coordinate [m]

1 Introduction

Nowadays there is an increasing demand of high performance rotating machine capable to run at high speed. To operate at such conditions accurate manufacturing, continuous monitoring and control of vibration levels are needed. In this context, growing attention has been paid to the design of relatively new active devices able to control vibrations and improve the dynamic behavior of machinery. Many authors have proposed different types of active devices, i.e. magnetic bearings [1], piezoelectric bearing pushers [2], hydraulic actuator journal bearings

[3], variable impedance bearings [4], active journal bearings with flexible sleeves [5], active lubricated bearings [6, 7], among others. Active gas bearings are presented as a solution for modern turbo-machinery applications where efficient performance at high speeds and clean environments are required. By using an active gas bearing it is possible to avoid the normal drawback of gas bearings, like poor carrying capacity and low damping, which often lead to a reduced range of stability. The first active gas journal bearing was presented by Horikawa and Shimokohbe [8]. In their prototype four pads were connected to the bearing housing through elastic hinges, in which piezoelectric actuators are fitted. Thus, measurements of the radial position of the shaft are sent to a control system which acts by sending a control signal to the actuators, which effectively work by modifying the fluid film thickness profile. Different methods to control the pressure distribution in the air gap of the thrust bearing have been studied, from controlling the feeding pressure [9] to modifying the shape of the bearing gap, either by acting locally around the restrictor [10] or by acting on the periphery of the bearing plate and modifying the conicity [11]. In relation with radial gas bearings, Morosi and Santos [12] proposed a modified form of the compressible Reynolds equation, coupled with a dynamic model of the piezoelectric injection system, to represent a hybrid gas bearing with four controllable radial injectors. Using this model they theoretically designed a PD control for a two degrees of freedom system, showing that it is possible to reduce the synchronous vibration components and also increase the stability range of the bearing. The same authors [13] presented the implementation of a PD controller of a rotor-gas bearing system based on experimental tuning of the control gains based on experimental waterfall diagrams. They presented an experimental validation using two piezoactuators to control the active forces in the horizontal direction, where the controller is able to effectively reduce the lateral vibrations in both directions. Qiu et al. [14] presented an experimental study, where a PID control is implemented, the active gas bearing is a tilting-pad type with embedded piezoelectric actuators, they results show that the self-excited vibration can be effectively suppressed if the gains of the controller are properly tuned. In [15] Theisen et al. identified a reduced model for the same system studied in [13], using grey box identification tools. Based on the reduced model identified and the pole placement method an effective state feedback controller was designed, able to significantly increase the damping factor of the rotor-bearing system. In contrast to [15], the main contribution of this paper is related to the theoretical design of PD controllers for rotor-bearing system presented in [13, 15] based on a mathematical model anchored to physical laws instead of experimental identification procedures. The system lateral dynamics are described using the modified version of the Reynolds equation, which accommodates the controllable annular injection [16], coupled to a finite element model of the flexible rotating shaft. To design the PD controller, the mathematical model is reduced using modal truncation. Experimental results show clearly the effectiveness of model-based control design approach.

2 Experimental set-up

The test rig used in this paper was firstly presented by Morosi and Santos [13] and it is schematically represented in Figure 1. The system consists of a rotor supported by two types of bearings, a ball bearing and a gas bearing. The rotor is driven by a gas turbine and the torque from the turbine is transmitted to the shaft with the aid of a flexible coupling. A rigid disc is attached to the end of the shaft, and two inductive proximity sensors are fixed to the holder around the disc.

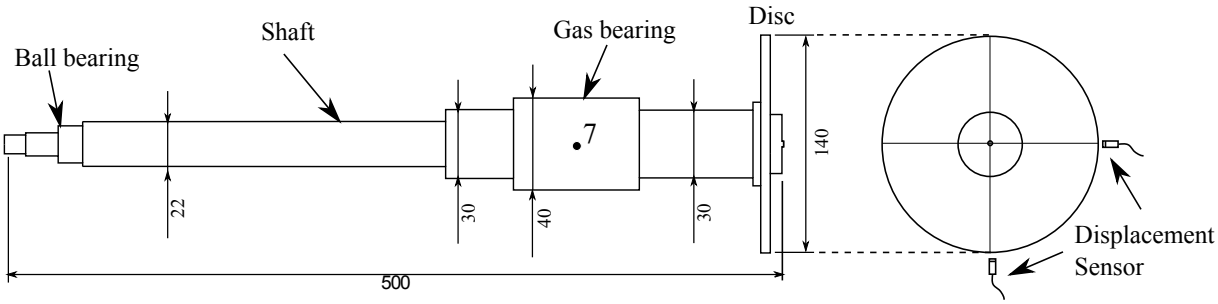

Figure 1: Flexible shaft and disc dimensions in mm, with the position of the two bearings and displacement sensors.

2.1 Gas journal bearing injection system.

The gas journal bearing injection system consists of three main parts, as it is illustrated in Figure 2(a); an aluminium housing **1**, a bronze sleeve **2**, and four adjustable injectors subsystems **3**. One of these injection subsystems is presented in detail in Figure 2(b). The piezo-actuator **5** pushes the plastic pin **6** in the direction of the gas bearing centre. The piezo-actuator is not capable of pulling the pin back, therefore a Belleville washer **7** is used. An O-ring seal is used to ensure that the pressurized air escapes only through the orifice, and a metallic structure **4** is used to support the whole actuation system. The orifices have a diameter of 2 mm and each of the injection orifices is fed by pressurized air from a compressed air network with a maximum supply pressure of $P_{sup} = 8$ bar. A detailed view of the injection zone is presented in Figure 2(c), where it can be seen that the vertical movement of the plastic pin pushed by the piezoactuator is capable to change the distance d, closing the area of injection, hence reducing the injected air flow. The initial distance d is set to 45 µm for the four injectors.

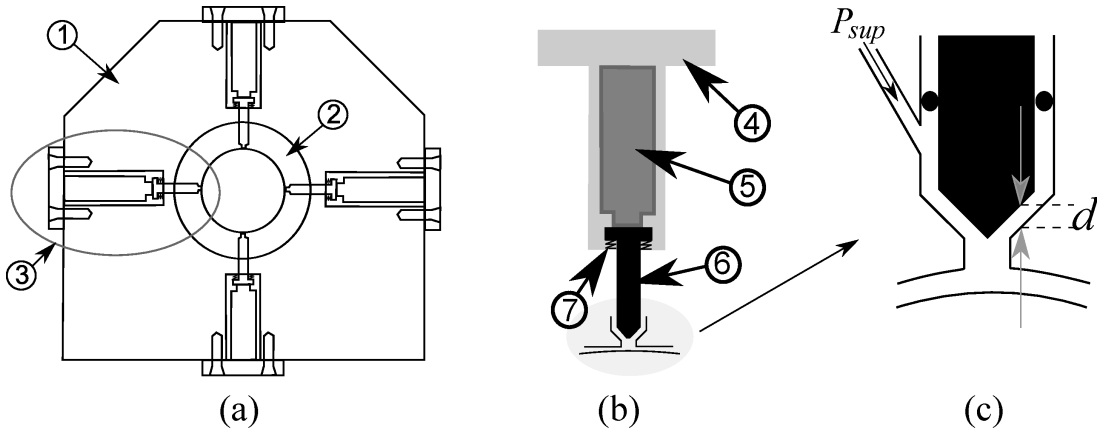

Figure 2: Gas bearing system - (a) scheme illustrating the hybrid gas bearing and its main components: aluminium housing **1**, bronze sleeve **2**, and adjustable injectors **3**; (b) schematic view of the assembling of the main parts of the adjustable gas bearing injection system, piezo-actuator **5**, plastic pin **6**, Belleville washer **7**, and aluminium support **4**; (c) Zoom view of the plastic pin interaction with the rotor.

3 Mathematical modelling

For the mathematical model of the rotor-bearing system, a finite element method (FEM) approach is followed. The rotor is modelled as a flexible shaft using 17 elements, where lateral and angular movements are considered, but structural damping is neglected. The disc is considered a rigid element, whose dynamics are incorporated into the model by adding mass and inertia to the respective node. The bearings are modelled as linear forcing elements acting on the rotor. Superimposing the mass, stiffness and gyroscopic matrices of each element of the shaft, without considering the gas bearing, one arrives at the global system of equations of the rotor:

$$\mathbf{M}\ddot{\mathbf{q}}(t) + \mathbf{D}\dot{\mathbf{q}}(t) + \mathbf{K}\mathbf{q}(t) = \mathbf{Q} \tag{1}$$

3.1 Controllable gas bearing

The controllable gas bearing is located in node 7 (see Figure 1). The interaction between the rotor and the bearings can be included into the model through linear dynamic coefficients of the gas film. To obtain these dynamic coefficients, it is necessary to calculate the pressure profile in the bearing surface, by solving the Reynolds equation according to the procedure described by Morosi and Santos [16]. In order to include an external injection of air, the Reynolds equation is modified. The injection flow is considered to be laminar, incompressible and fully developed and as such is described by the Hagen-Poiseuille formula for an annular flow. Density changes along the injector are considered to be negligible. The resulting equation of the injection flow is given by Eq. (2).

$$V_{inj}(y,z,t) = -C_d \frac{1}{4\mu}\left(\frac{\partial p(y,z,t)}{\partial x}\right)\left[\left\{\frac{{d_0}^2}{4} - \frac{d(y,z)^2}{4}\right\} - \left\{\frac{{d_0}^2}{4} - \frac{{d_{int}}^2}{4}\right\}\frac{\ln(d_0/d(y,z))}{\ln(d_0/d_{int})}\right] \tag{2}$$

Where C_d is a discharge coefficient. The value of this coefficient is obtained from a computational fluid dynamic (CFD) model and experimental analysis [17], where it is demonstrated that this assumption leads to good results for steady state conditions. This extra term is added to the general formulation of the compressible Reynolds equation in the orifice region. The new modified Reynolds equation (MRE) is defined in Eq. (3).

$$\frac{\partial}{\partial y}\left[\frac{ph^3}{\mu}\frac{\partial p}{\partial y}\right] + \frac{\partial}{\partial z}\left[\frac{ph^3}{\mu}\frac{\partial p}{\partial z}\right] = 6U\frac{\partial}{\partial y}(ph) + 12\frac{\partial(ph)}{\partial t} + 12pV_{inj}(y,z,t) \tag{3}$$

The pressure distribution in the bearing is continuous in the circumferential coordinate and equal to the atmospheric value (P_{atm}) at the bearing edges. The boundary conditions for the steady-state Eq. (4), are defined by:

$$\begin{aligned} p_0(y,0) &= p_0(y,L) = P_{atm} \\ p_0(0,z) &= p_0(2\pi R,z) \\ \frac{\partial p_0(0,z)}{\partial y} &= \frac{\partial p_0(2\pi R,z)}{\partial y} \end{aligned} \tag{4}$$

For a given operation condition and initial eccentricity, the nonlinear partial differential equation (PDE) Eq. (3) is solved using a finite difference approximation on a discretized domain. The pressure field is integrated over the bearing surface, which in turn imposes vertical and horizontal lubrication reaction forces. Expressions for the static and dynamic pressure equations are derived with a perturbation method, as introduced by Lund [18]. The solution of the first-order perturbation equations for the perturbed pressures (p_X, p_Y) is straightforward, as these are linear PDEs. Given a zeroth order field p_0, they are solved via a finite difference scheme and subsequently integrated over the bearing surface to determine the stiffness and damping coefficients.

$$\mathbf{K}^H + i\omega\mathbf{D}^H = \int_0^L\int_0^{2\pi}\begin{bmatrix} p_X\cos\Omega & p_X\sin\Omega \\ p_Y\cos\Omega & p_Y\sin\Omega \end{bmatrix} Rd\Omega dz \tag{5}$$

It is important to notice that the dynamic coefficients are dependent on the excitation frequency and that the model assumes small amplitude of perturbations. Including the $\mathbf{K}^H$ and $\mathbf{D}^H$ from the gas bearing in the Eq. (5) and writing in state space form the Eq. (6) is found:

$$\underbrace{\begin{bmatrix}\dot{\mathbf{q}}(t)\\ \ddot{\mathbf{q}}(t)\end{bmatrix}}_{\dot{\mathbf{z}}(t)} + \underbrace{\begin{bmatrix}\mathbf{0} & \mathbf{I}\\ \mathbf{M}^{-1}(\mathbf{K}+\mathbf{K}^H) & \mathbf{M}^{-1}(\mathbf{G}+\mathbf{D}^H)\end{bmatrix}}_{\mathbf{A}}\underbrace{\begin{bmatrix}\mathbf{q}(t)\\ \dot{\mathbf{q}}(t)\end{bmatrix}}_{\mathbf{z}(t)} = \underbrace{\begin{bmatrix}\mathbf{0}\\ \mathbf{M}^{-1}\mathbf{F}(t)\end{bmatrix}}_{\mathbf{f}(t)}$$

$$\dot{\mathbf{z}}(t) + \mathbf{A}\mathbf{z}(t) = \mathbf{f}(t) \tag{6}$$

The homogenous case is considered, with $\mathbf{f}(t) = \mathbf{0}$, and varying the angular velocity from 0 Hz up to 300 Hz (18000 rpm), in Figure 3(a) the system eigenvalues are calculated for each frequency (Campbell diagram). Figure 3(b) shows the damping factors for the four first modes for the same angular velocities illustrated in the Campbell diagram. From Figures 3(a) and 3(b) it is possible to conclude that from the viewpoint of improving the machine performance, it is important to increase the damping of the first two modes which is the aim of the active control system propose in this work.

4 Control system design

The active fluid film forces $\mathbf{f}(t)$ can be defined proportional to the applied voltage $\mathbf{u}(t)$ and the state-space Eq. (6) rewritten as:

$$\dot{\mathbf{z}}(t) = \mathbf{A}\mathbf{z}(t) + \mathbf{B}\mathbf{u}(t) \tag{7}$$

$$\mathbf{y}(t) = \mathbf{C}\mathbf{z}(t) \tag{8}$$

where $\mathbf{B}$ it is the matrix which relates the input voltage signal $\mathbf{u}(t)$ with the actuator force $\mathbf{f}(t)$.

4.1 Determination of the control matrix B

To obtain the matrix $\mathbf{B}$ a pseudo-static testing is performed. It is assumed that the results obtained for the static case analysis will be useful for the low angular velocity cases, because in these conditions the aerostatic effect is predominant. For a given condition ($P_{sup} = 8$ bar, angular velocity $\Omega = 0$ Hz and input voltage $u_x = u_y = 0$), the rotor position ($\mathbf{y}_0 = [e_{x0}, e_{y0}]$) is measured. External static loads on the rotor are applied by means of passive magnets, leading to a change in journal equilibrium position. By varying the input signal $\mathbf{u}(t)$ to the actuators, active forces are generated repositioning the rotor into the original equilibrium position $\mathbf{y}_0$. The static test is repeated with several values of static loads and the input voltage recorded. In this manner the four coefficients of $\mathbf{B}^*$ ($B_{xx}, B_{xy}, B_{yx}, B_{yy}$) can be experimentally obtained. The results are illustrated in Figure 4. It is also assumed, for simplicity, that the active forces in the orthogonal directions are uncoupled, i.e. B_{xy} and B_{yx} are negligible. So $\mathbf{B}^*$ it is defined as:

$$\mathbf{B}^* = \begin{bmatrix} \mathbf{0}_{24\times1} & \mathbf{0}_{24\times1} \\ B_{xx} & B_{xy} \\ B_{yx} & B_{yy} \\ \mathbf{0}_{46\times1} & \mathbf{0}_{46\times1} \end{bmatrix}_{72\times2} \tag{9}$$

where B_{yy}= 11 N/V , B_{xx}= 9.2 N/V, $B_{xy} = B_{yx}$= 0 N/V and $\mathbf{B}$ is finally defined as:

$$\mathbf{B} = \begin{bmatrix} \mathbf{0} \\ \mathbf{M}^{-1}\mathbf{B}^* \end{bmatrix}_{144\times2} \tag{10}$$

The efficiency of the piezoactuator and consequently of the control system, is strongly affected by the piezoactuator dynamics when the excitation frequency is near the piezoactuator natural frequency (10 kHz), nevertheless in the range of frequencies studied in this work, the value of $\mathbf{B}$ is hardly dependent of the frequency, for that reason the matrix $\mathbf{B}$ is considered constant.

4.2 Model reduction and complex separation

For control purposes the system is reduced, using pseudo-modal reduction and using complex term separation techniques to avoid complex eigenvalues. These procedures are performed according to Christensen and Santos [19]. The new reduced system has four degrees of freedom and leads to a very good estimation of the response for the two lowest modes.

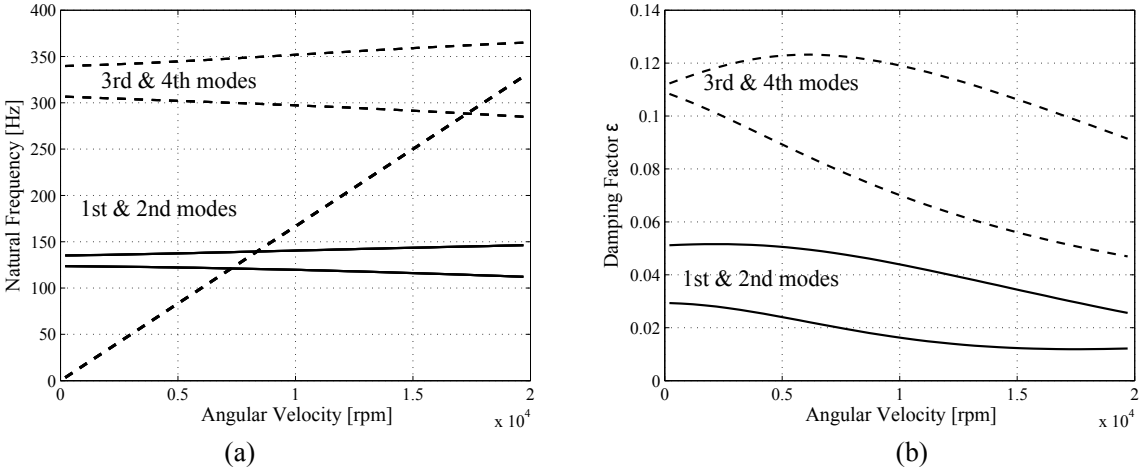

Figure 3: First four eigenvalues of the rotor-bearing system: (a) Campbell diagram and (b) damping factor.

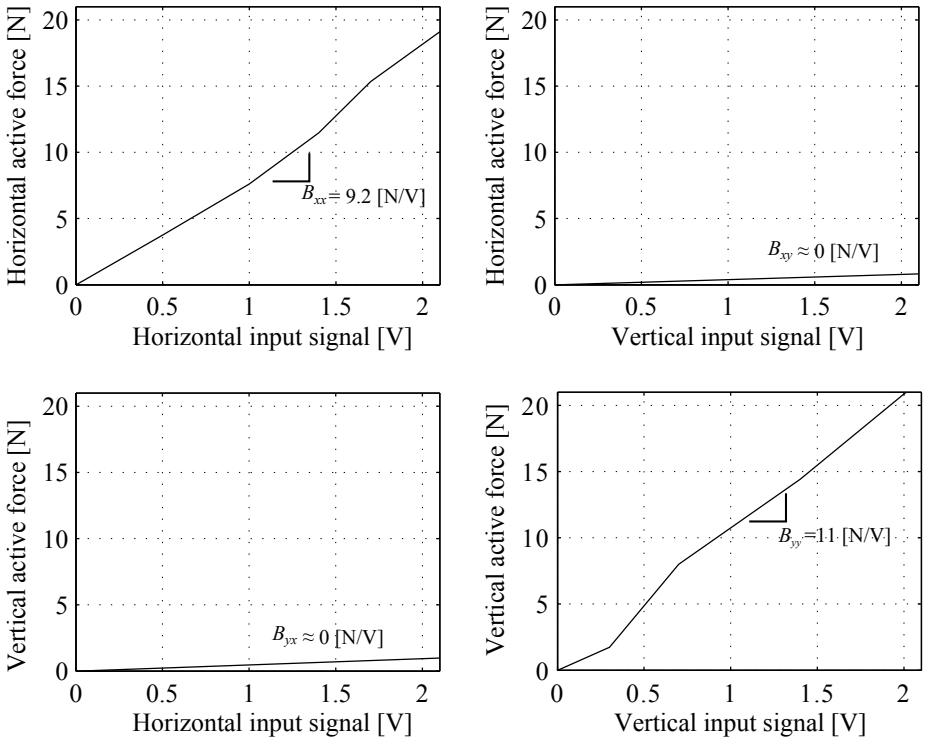

Figure 4: Experimental characterization of active air forces - Force versus piezoelectric voltage for the case of no rotor angular velocity and 8 bar of injection pressure.

4.3 Implementation of PD control

The simplest form of the PD control algorithm is given by:

$$\mathbf{u}(t) = K_p \cdot \mathbf{e}(t) + K_d \cdot \dot{\mathbf{e}}(t) \tag{11}$$

where the subscripts p and d refer to the proportional and derivative gain respectively. From a practical point of view, implementation of the above algorithm has certain limitation. Ideal derivative has very high gain for high frequency signals. This means that high frequency measurement noise will generate large variations of the control signal. The effect of measurement noise can be reduced by adding a first order low pass filter to the derivative term [20]. The PD algorithm can be written as:

$$\mathbf{u}(s) = \left(K_p + \frac{K_d \cdot N}{1 + N/s} \right) \cdot \mathbf{e}(s) \tag{12}$$

where N is the constant which defines the low pass filter cut-off frequency.

4.4 PD control tuning

The main goal of the controller is to increase the damping factor associated with the two lowest modes. Tuning is performed in order to investigate the influence of the proportional and derivative gains on the damping factor related with the lowest modes. The outcome of such analysis for one particular operational condition is presented in Figure 5, where the colors represent the values of damping factors associated with the first mode shape in vertical direction. In this case the operational conditions are: zero angular velocity and injection pressure of 8 bar. From Figure 5 it can be said that a negative derivative gain produces an unstable response of the rotor-bearing system. An improvement of the dynamic properties can be achieved, using different combinations of the values for proportional and positive derivative gains. To avoid the problems related with the amplification of noise, the case with derivative gain equal to zero is chosen. In Figure 6 the damping factor associated with the two first modes shapes is presented for the case with only proportional gain. From this figure is clearly seen that for the two modes

there is a limited range where the system has a higher damping factor than the case with no controller, -2.4×10^5 to 1.1×10^5 V/m in vertical direction and -2.5×10^5 to 1.0×10^5 V/m in horizontal direction. In Figures 5 and 6 there are four letters (A, B, C and D) showing the cases here studied. In case A the proportional gain is equal to 2×10^5 V/m and for both modes the system becomes unstable; the case B represent the case with no control action; cases C and D produces a more damped and stable system than the case B, using proportional gains equal to -1×10^5 V/m and -1.5×10^5 V/m respectively.

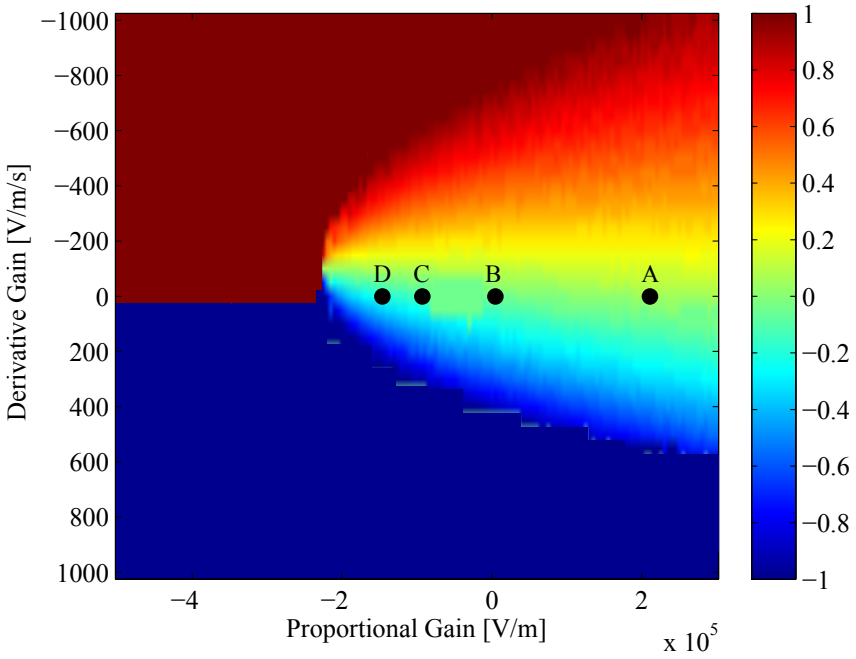

Figure 5: Damping factor associated with the first mode shape as a function of the proportional gain K_p and derivative gain K_d. Zero angular velocity and injection pressure of 8 bar.

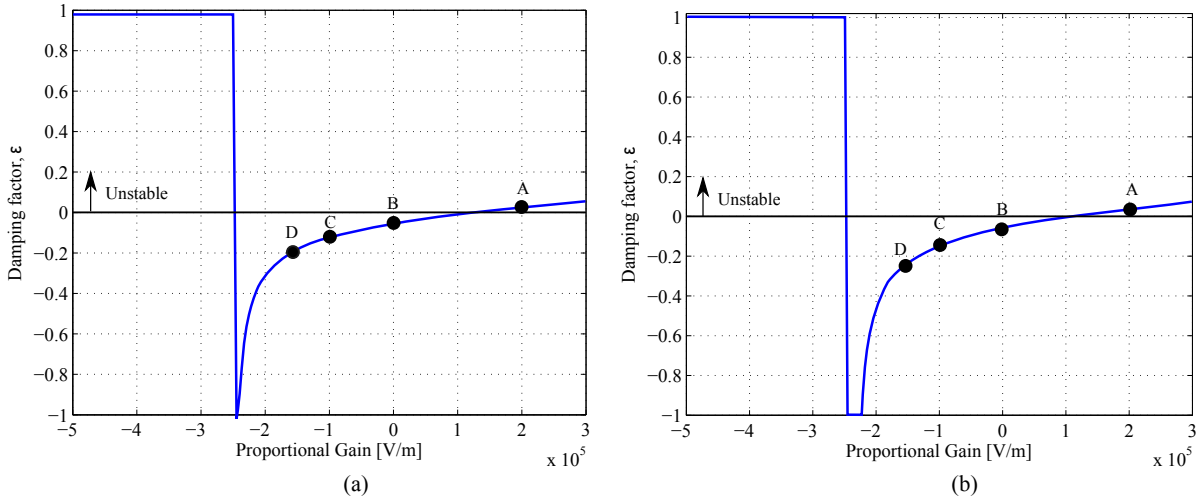

Figure 6: Damping factor associated with the first mode shape as a function of the proportional gain K_p - (a) vertical direction, (b) horizontal direction. Zero angular velocity and injection pressure of 8 bar.

5 Results

The controller performance is evaluated for different operational conditions (0 rpm, 2000 rpm and 4000 rpm) and using three values of proportional control gain (cases A, C and D from Figures 5 and 6) taking into account the rotor- bearing system time response to an impulsive force and comparing the damping associated with the first two mode shapes, theoretically and experimentally. The injection pressure for this analysis is 8 bar. In Figures 7 the theoretical time response to and impulsive exitacion is presented for one particular condition of angular velocity (0 rpm) and for the cases C and D with proportional gain -1×10^5 V/m and -1.5×10^5 V/m. In Figure 8 the experimental impulsive response for the same conditions is presented. From Figure 7 and 8 it is evident that the

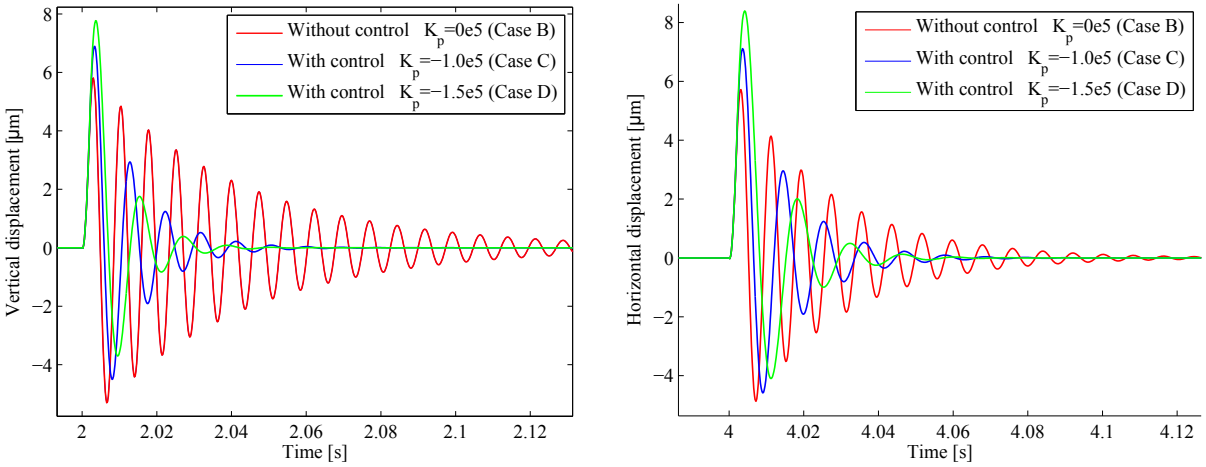

Figure 7: Theoretical results - Impulsive response of the rotating disc in time domain: without control (red), with control case C (blue) and with control case D (green).

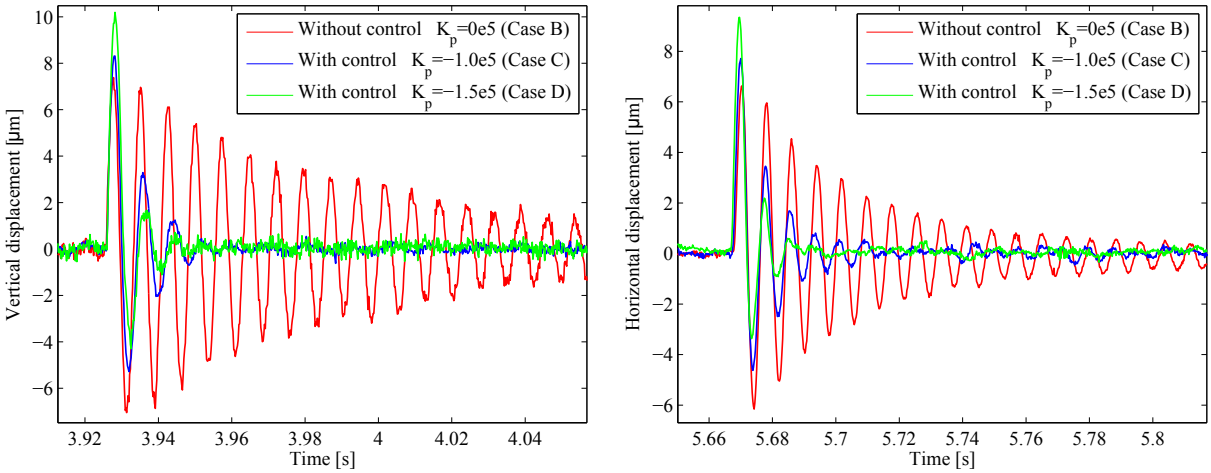

Figure 8: Experimental results - Impulsive response of the rotating disc in time domain: without control (red), with control case C (blue) and with control case D (green).

controller allows for a significant damping increase and that the experiments are in good correlation with the theory. In Table 1 and 2 the theoretical and experimental damping factor are presented for all the conditions studied. In Figure 9 the time response for the case A, when the proportional gain is equal to 2×10^5 V/m, is illustrated. It can be seen that, as it is expected, the system becomes unstable and the response shows and exponential increase in the level of vibrations until the actuator saturation is reached.

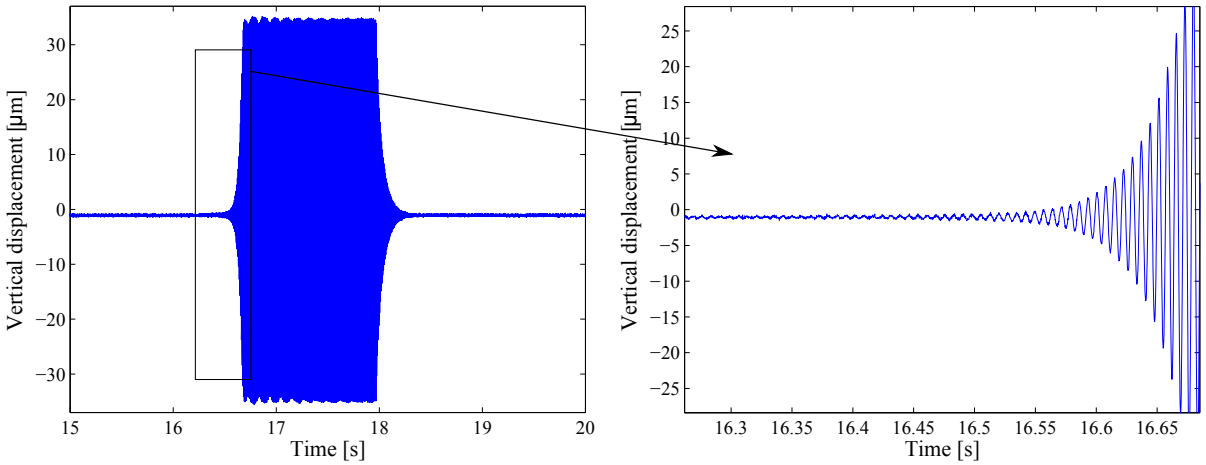

Figure 9: Experimental results - System response in time domain for $K_p = 2 \times 10^5$ V/m, Case A - left hand side: displacement of the disc, right hand side: zoomed view.

Table 1: Damping factors at different angular velocity Ω and proportional gain K_p - Theoretical results.

	Ω=0 rpm			Ω=2 krpm		Ω=4 krpm	
Direction	Case B	Case C	Case D	Case C	Case D	Case C	Case D
Vertical	0.029	0.103	0.167	0.099	0.159	0.091	0.146
Horizontal	0.051	0.137	0.219	0.139	0.227	0.142	0.231

Table 2: Damping factors at different angular velocity Ω and proportional gain K_p - Experimental results.

	Ω=0 rpm			Ω=2 krpm		Ω=4 krpm	
Direction	Case B	Case C	Case D	Case C	Case D	Case C	Case D
Vertical	0.025	0.131	0.214	0.153	0.215	0.157	0.280
Horizontal	0.050	0.157	0.208	0.119	0.210	0.120	0.220

6 Conclusion and future work

In the present study, a model-based controller is designed for an actively-lubricated air bearing based on the modified Reynolds equation. The rotor-bearing model is capable to capture the system dynamics accurately, but small deviations between model and physical system are still visible. Such deviations come fundamentally from the complex behavior of fluid film flow interacting with the injection flow and the simplifying assumptions used, mainly in the derivation of the control matrix $\mathbf{B}$. With the aim of increasing damping, a proportional controller is designed and experimentally implemented. The controller allows for significant increase in damping for a proportional gain $K_p = -1 \times 10^5$ V/m the damping increases almost 4 times and for $K_p = -1.5 \times 10^5$ V/m almost 6 times. Experimental results allows for validation of the theoretical model showing that the differences are less than a 50% for all the conditions of velocity and proportional gains studied. The theoretical and experimental results clearly show the advantage of applying control techniques to gas bearings. Future work involves: a) more accurate modelling of fluid film dynamics, b) theoretical derivation of matrix $\mathbf{B}$ is necessary to improve the model-based control design approach and (c) study of the influence of quantity and position of orifices in the bearing surface, in the dynamical behavior of the rotor-bearing system.

REFERENCES

[1] E. Maslen, *Magnetic bearings - theory, design and application to rotating machinery*. New York, USA, Springer, 2009.

[2] A. B. Palazzolo, R. M. Alexander, and J. Montague, "Piezoelectric Pushers for Active Vibration Control of Rotating Machinery," *Journal of Vibration, Acoustic, Stress and Reliability in Design*, vol. 111, no. July 1989, pp. 298–305, 1989.

[3] I. F. Santos, "On the Adjusting of the Dynamic Coefficients of Tilting-Pad Journal Bearings," *Tribology Transactions*, vol. 38, pp. 700–706, Jan. 1995.

[4] P. J. Ogrodnik, M. J. Goodwin, and M. P. Roach, "A novel variable impedance hydrodynamic oil-film bearing Part 1 : theoretical modelling," *Proceedings of the Institution of Mechanical Engineers , Part J : Journal of Engineering Tribology*, 1996.

[5] L. Sun and J. Krodkiewski, "Experimental Investigation of Dynamic Properties of an Active Journal Bearing," *Journal of Sound and Vibration*, vol. 230, pp. 1103–1117, Mar. 2000.

[6] F. H. Russo and I. F. Santos, "Tilting-Pad Journal Bearings With Electronic Radial Oil Injection," *Journal of Tribology*, vol. 120, no. 3, pp. 583–594, 1998.

[7] I. F. Santos, R. Nicoletti, and A. Scalabrin, "Feasibility of Applying Active Lubrication to Reduce Vibration in Industrial Compressors," *Journal of Engineering for Gas Turbines and Power*, vol. 126, no. 4, p. 848, 2004.

[8] O. Horikawa, K. Sato, and A. Shimokohbe, "An active air journal bearing," *Nanotechnology*, vol. 3, pp. 84–90, 1992.

[9] F. Al-Bender, "On the modelling of the dynamic characteristics of aerostatic bearing films: From stability analysis to active compensation," *Precision Engineering*, vol. 33, pp. 117–126, Apr. 2009.

[10] H. Mizumoto, S. Arii, Y. Kami, and K. Goto, "Active inherent restrictor for air-bearing spindles," *Precision Engineering*, vol. 19, pp. 141–147, 1996.

[11] G. Aguirre, F. Al-Bender, and H. V. Brussel, "Dynamic stiffness compensation with active aerostatic thrust bearings," in *Proceedings of ISMA 2008*, pp. 105–118, 2008.

[12] S. Morosi and I. F. Santos, "Active lubrication applied to radial gas journal bearings. Part 1: Modeling," *Tribology International*, vol. 44, pp. 1949–1958, Nov. 2011.

[13] S. Morosi and I. F. Santos, "Experimental investigations of active air bearings," in *ASME turbo Expo 2012*, pp. 1–10, 2012.

[14] J. Qiu, J. Tani, and T. Kwon, "Control of Self-Excited Vibration of a Rotor System With Active Gas Bearings," *Journal of Vibration and Acoustics*, vol. 125, no. 3, p. 328, 2003.

[15] L. R. Theisen, F. G. Pierart, H. Niemann, I. F. Santos, and B. Mongens, "Experimental Grey box model identification and control of an active gas bearing," in *Vibration Engineering and Technology of Machinery* (J. K. Sinha, ed.), vol. 23 of *Mechanisms and Machine Science*, ch. Mechanisms, pp. 963–976, Springer International Publishing, 23 ed., 2015.

[16] S. Morosi and I. F. Santos, "On the modelling of hybrid aerostatic-gas journal bearings," *Proceedings of the Institution of Mechanical Engineers, Part J: Journal of Engineering Tribology*, vol. 225, pp. 641–653, June 2011.

[17] F. G. Pierart and I. F. Santos, "Steady state characteristics of an adjustable hybrid gas bearing - CFD, modified Reynolds equation and experimental validation," *Journal of Engineering Tribology*, vol. (submitted), 2015.

[18] J. W. Lund, "Calculation of Stiffness and Damping Properties of Gas Bearings," *Journal of Lubrication Technology*, vol. 90, no. 4, p. 793, 1968.

[19] R. Christensen and I. Santos, "Design of active controlled rotor-blade systems based on time-variant modal analysis," *Journal of Sound and Vibration*, vol. 280, pp. 863–882, Feb. 2005.

[20] A. J. Isaksson and S. F. Graebe, "Derivative filter is an integral part of PID design," *IEE proc.-Control Theory Appl.*, vol. 149, no. 1, pp. 41–45, 2002.